Applied Surface Science 283 (2013) 402–410

Contents lists available at SciVerse ScienceDirect

Applied Surface Science

journal homepage: www.elsevier.com/locate/apsusc

One-step solvothermal synthesis of hierarchically porous nanostructured CdS/TiO_2 heterojunction with higher visible light photocatalytic activity

Guidong Yang[a,*], Bolun Yang[a], Tiancun Xiao[b,*], Zifeng Yan[c]

[a] Department of Chemical Engineering, School of Chemical Engineering and Technology, Xi'an Jiaotong University, Xi'an, 710049, China
[b] Department of Chemistry, Inorganic Chemistry Laboratory, University of Oxford, Oxford, OX1 3QR, UK
[c] State Key Laboratory for Heavy Oil Processing, China University of Petroleum, Qingdao, 266555, China

ARTICLE INFO

Article history:
Received 11 April 2013
Received in revised form 21 June 2013
Accepted 22 June 2013
Available online 1 July 2013

Keywords:
One-step synthesis
Hierarchical
Heterojunction
CdS/TiO_2
Photocatalysis
Visible-light

ABSTRACT

One-step solvothermal method was developed for the synthesis of hierarchically porous nanostructured CdS/TiO_2 heterojunction materials, which exhibited enhanced visible-light-driven photocatalytic activity in decomposing both methyl orange (MO) and rhodamine B (RhB) in water. The photocatalyst with the highest performance was the one prepared using the Ti:Cd molar ratio of 1:1. Based on the characterization results of XRD, XPS, FT-IR, SEM, HRTEM, UV–vis DRS and N_2 adsorption–desorption, the influence of coupling TiO_2 with CdS on the crystal phase, band structure, surface element composition, morphology, optical absorption and surface area of the as-prepared samples are investigated. The results showed that the CdS/TiO_2 heterojunction catalysts possessed well-defined hierarchically porous structure composed of anatase TiO_2 and hexagonal CdS nanoparticle with average grain size of 4–6 nm. Their enhanced catalytic activity can be attributed to the synergistic effect of crystal compositions, porous architectures, electronic band structure, large specific surface area and strong visible light absorption.

1. Introduction

The photocatalytic degradation of organic pollutants using oxide semiconductor nanoparticles as a photocatalysts has attracted much attention due to its good ability to broaden compound applicability and low cost [1–3]. Titanium oxide (TiO_2), a well-known photocatalyst, has been studied extensively for application in the field of environmental purification, solar energy conversion and hydrogen generation [4–6]. However, a critical drawback is that the relatively large band gap of titania (3.2 eV for anatase and 3.0 eV for rutile), which is too large to allow efficient absorption of most sunlight. On the other hand, a high photogenerated electrons and holes recombination rate also greatly reduces the quantum efficiency of titania. Consequently, these two main disadvantages are unfavorable for the enhancement of photocatalytic activity and limit the large-scale application of the pure TiO_2 in solar-driven water purification [7–10].

In order to utilize a larger portion of solar energy, particularly the visible light band, which accounts for more than 40% of the incoming solar energy on the earth's surface, great efforts have been made in exploring various new visible-light-driven TiO_2-base photocatalysts in the past decade. Accordingly, a variety of strategies, such as doping with anion or cation [11,12], sensitizing with dyes [13] and combining with narrow band gap semiconductor [14,15], have been investigated to modify the TiO_2 photocatalyst. Among the modified photocatalysts, coupling of a narrow band gap semiconductor to form heterojunction is regarded as the most promising techniques for harvesting the most sunlight and the enhancement of quantum yield of TiO_2 [14–16]. It is known that an effective heterojunction system would have the matched band structure and requisite band energy [17]. A typical example is CdS/TiO_2 composite system [14,18], which shows stronger visible light absorption owing to the photosensitization of cadmium sulphide (CdS) with a direct band gap of around 2.42 eV [19]. In the meanwhile, because the conduction band of CdS is higher than that of TiO_2, the photogenerated electrons in CdS can be efficiently injected in TiO_2 when exposed to visible light irradiation, which enables the promotion of the separation of electron–hole pairs and increases quantum efficiency [18–20].

More recently, hierarchically porous semiconductor oxides with different ranges of pores have attracted increasing more attentions [21–23]. The presence of micropores (<2 nm) in hierarchical structure contributes to a greater specific surface area, which can offer large active sites to induce more surface absorbability of dye molecules, whilst the presence of mesopores (2–50 nm) can

* Corresponding author. Tel.: +86 29 82663189.
E-mail addresses: guidongyang@mail.xjtu.edu.cn (G. Yang), Xiao.tiancun@chem.ox.ac.uk (T. Xiao).

0169-4332/$ – see front matter © 2013 Elsevier B.V. All rights reserved.
http://dx.doi.org/10.1016/j.apsusc.2013.06.122

increase mass transport through the material and increase the available surface area. Recent progress shows that materials with hierarchically porous structures present significantly enhanced performance in photocatalysis compared with single-sized pores [23]. Hasegawa et al. [24] prepared monolithic titania with hierarchically porous structures via sol–gel route accompanied by phase separation utilizing a chelating agent and mineral salt. Pan et al. [25] reported that the hierarchically mesoporous F–TiO_2 hollow microspheres have been produced by hydrothermal treatment of TiF_4 in H_2SO_4 aqueous solution at 160 °C for 4 h. However, to date, very limited improvements are achieved for the synthesis of CdS/TiO_2 heterojunction with hierarchically porous nanostructure by a convenient way.

Here for the first time, we report a facile approach to prepare a novel hierarchically porous CdS/TiO_2 heterostructure photocatalyst using one-step solvothermal method at low temperature. The preparation conditions are much milder than those of conventional methods because of no need of the calcinations step during the synthesized process, which therefore avoid the particle aggregation and the collapse of the porous structure caused by calcinations at high temperature, as result of leading to the increase in photocatalytic efficiency. The photocatalytic activities were evaluated by the decomposition of both methyl orange and rhodamine B under visible light irradiation. The results showed that the as-obtained CdS/TiO_2 heterojunctions present strong visible light activity due to their hierarchical pores structure and electron–hole separating ability.

2. Experimental procedure

2.1. Materials and synthesis

All chemicals are of reagent grade and used without further purification. The fabrication of hierarchically porous CdS/TiO_2 heterostructure photocatalysts were simple achieved by one-step solvothermal method at low temperature. In a typical run of synthesis, 0.01 mol tetrabutyl titanate and 4 mL acetic acid were added dropwise to 15 mL ethanol with continuous stirring for 30 min to form a light yellow solution A. The desired amounts of cadmium chlorides and thiourea (the molar ratio of Cd to S was 1:1) were dispersed in 20 mL ethanol and vigorously stirred for 30 min to generate a white suspension B. Meanwhile, 4 g glucose was dissolved in 6 mL distilled water at 40 °C for 30 min to form solution C. Afterwards, solution C was added dropwise into suspension B and stirred for a further 30 min, and solution A was then added slowly into the above mixture with continuous stirring. The obtained final white suspension was then transferred into a Teflon-lined autoclave, maintained at 180 °C for 24 h. After reaction under self-generated pressure and cooling down to room temperature, the product was collected by filtration, washed with deionized water and ethanol and dried at 80 °C overnight. The as-prepared photocatalysts with different starting Ti:Cd molar ratios of 1:0.75, 1:1, 1:1.25 and 1:1.5 were denoted as CT-1, CT-2, CT-3 and CT-4, respectively. For comparison, pure TiO_2 and CdS samples were also prepared by the above method.

2.2. Characterization of materials

N_2 adsorption–desorption isotherms of catalysts were conducted at liquid nitrogen temperature in a Micromeritics ASAP 2020 instruments, the samples was degassed at 200 °C overnight before the actual measurement. The pore size distribution was calculated from desorption branch of the absorption isotherms using the Barrer–Joyner–Halenda (BJH) method and surface area was determined using BET method. The crystalline structure and phase component of the resulting CdS/TiO_2 materials were determined using X-ray diffraction with a Philips X'PeRT Pro Alpha 1 diffractometer with Cu Kα radiation (λ = 1.5406 Å) operated at a tube current of 40 mA and a voltage of 40 kV. Data were collected over 2θ values from 20° to 70°, at a scan speed of 2° min^{-1}. Diffuse reflectance UV–vis diffuse reflectance spectra (DRS) were measured on a Hitachi U-4100 instrument employed with a labsphere diffuse reflectance accessory. The product morphology was examined using field-emission scanning electron microscope (FESEM; JEOL, JSM-6700F, 5 kV) and transmission electron microscope (TEM; JEOL, JEM-2100F, 200 kV). Infrared absorption spectra were recorded using a Bruker Vertex-70 FT-IR spectrometer with KBr as the reference sample. The chemical forms of the products were studied using X-ray photoelectron spectroscopy (XPS) Axis Ultra, Kratos (UK) using monochromatic Al K_α radiation (150 W, 15 kV, 1486.6 eV). The vacuum in the spectrometer was 10^{-9} Torr. Binding energies were calibrated relative to the C 1s peak (284.8 eV) from hydrocarbons adsorbed on the surface of the samples.

2.3. Photocatalytic activity test

The photocatalytic activities of the hierarchically porous CdS/TiO_2 heterostructure photocatalyst were evaluated by the photodegradation of MO and RhB under visible light illumination. It is known that MO is a kind of stable azo dye, and RhB is one of the most commonly used xanthenes dyes. Both of the representative dyes are widely used in various industrial applications and also have a good stability in aqueous solutions, and therefore severe environmental problems are easily caused by these dye effluents. In this work, the photocatalytic reactions were conducted in an open reactor with a cooling-water-cycle system keeping the reaction temperature constant. The light source was a 300 W Xenon lamp (Nbet, HSX-F/UV300, Beijing, China), emitting UV and visible light simultaneously. For visible light measurements, a 420 nm cut-off glass filter was mounted before the output of light source to remove UV light and admit only visible light to enter into the reactor and the light intensity was 28 mW/cm^2. Then 100 mg of CdS/TiO_2 heterojunction sample was suspended in 100 mL of methyl orange (10 mg/L) solution and rhodamine B (20 mg/L), respectively. Before the photoreaction, the suspension was stirred in the dark for 120 min to make sure the mixture had achieved adsorption/desorption equilibrium, then 3 mL of the solution was taken from the reactor in a constant time during the photoreaction. The sample powder was separated from the solution by a centrifugation method, and the concentration of the remaining MO and RhB liquid was determined by UV–vis spectrophotometer.

For the measurements of the repeated photoactivity experiment: 0.05 g CT-2 sample was dispersed in 50 mL RhB solution (20 mg/L) and the photoreaction performed as described above, but the photoreaction time is certain for 100 min. After each run of reactions, the CT-2 sample was separated from the solution, washed and dried overnight at 80 °C. Then, the separated CT-2 sample was returned to the photocatalytic reaction system, and each recycling test is conducted under the same conditions.

3. Results and discussion

Fig. 1 shows the XRD patterns of as-synthesized CdS/TiO_2 heterojunction samples with different Ti:Cd molar ratios. The main peaks located at 24.83, 26.53, 28.22, 36.66, 43.74, 47.89, and 51.89° 2θ were assigned to the (1 0 0), (0 0 2), (1 0 0), (1 0 2), (1 1 0), (1 0 3) and (1 1 2) planes of the hexagonal structure of CdS (JCPDS card no. 77-2306) [26,27]. Besides the characteristic signals corresponding CdS, three extra weak peaks at 37.38°, 54.75° and 62.19° 2θ were observed in the XRD profiles of CdS/TiO_2 heterojunction, which can

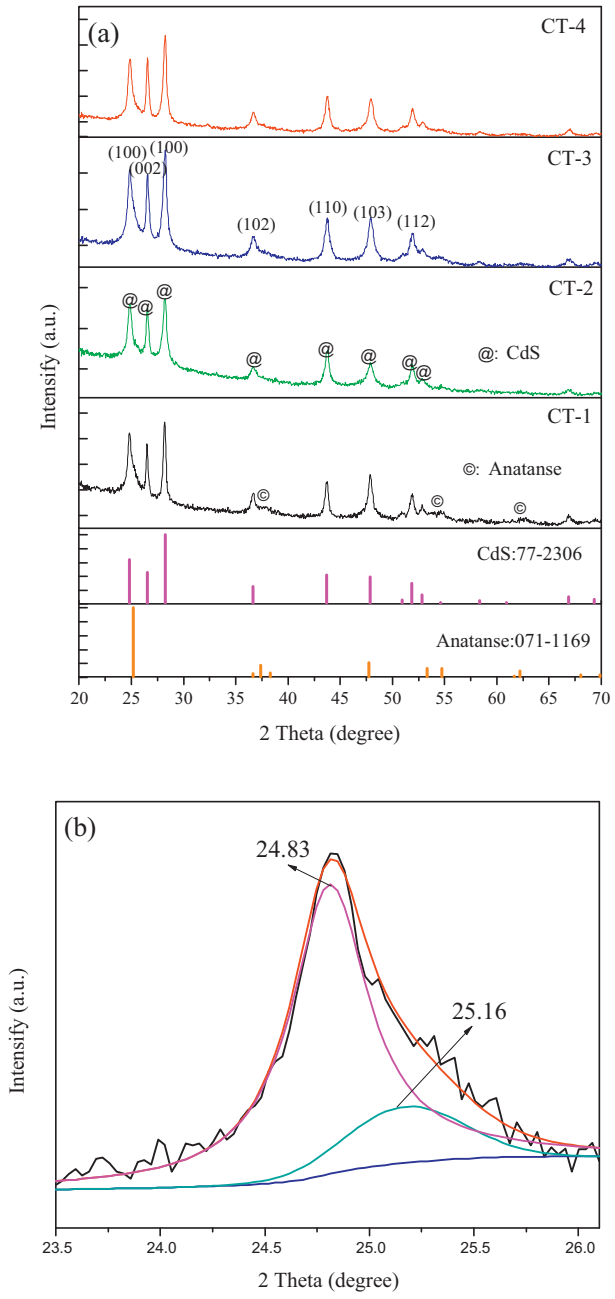

Fig. 1. (a) XRD patterns of the hierarchically porous CdS/TiO_2 heterojunction samples with different Ti:Cd molar ratios and (b) the magnification of the diffraction peak around 25.0°.

be indexed to the (0 0 4), (2 1 1) and (2 0 4) planes of the anatase structure of TiO_2 [28]. The XRD peak of anatase (1 0 1) TiO_2 cannot be found in XRD patterns, this maybe ascribe to the overlapping between anatase (1 0 1) TiO_2 and hexagonal (1 0 0) CdS because the positions of these two peaks are quite similar. In addition, it can be observed that the principal diffraction peak around 25.0° 2θ for all CdS/TiO_2 samples is somewhat asymmetric, suggesting that there are at least two kinds of crystalline phase existing in the samples. Fig. 1(b) shows the magnification of the diffraction peak around 25.0°, and the curve fitting patterns are also shown in Fig. 1(b). The peak at 24.83° is due to the (1 0 0) plane of the hexagonal CdS, and the signal at 25.16° is assigned to the (1 0 1) diffraction peak of anatase TiO_2. This finding further confirms the co-existence of CdS and TiO_2 phase in the obtained hierarchically porous CdS/TiO_2 heterojunction. No significant shift of principal peaks of either the CdS or the TiO_2 was observed, indicating that the CdS was present in a separated phase rather than in the TiO_2 lattice.

Table 1
Pore characteristics and surface area of the representative CdS/TiO_2 heterojunctions.

Samples	BET (m^2/g)	Pore volume (cm^3/g)	Average pore size (nm)
CT-2	134.9	0.159	4.25
CT-4	90.6	0.134	5.18

The nitrogen adsorption–desorption isotherms and the corresponding pore size distributions curve of the hierarchically porous CdS/TiO_2 heterojunction samples are shown in Fig. 2. According to the IUPAC classification [29,30], the adsorption isotherms of both CT-2 and CT-4 show the typical IV isotherm, indicative of a characteristic mesoporous structure of solid. Moreover, a clear absorption hysteresis loop located at $0.40 < P/P_0 < 0.94$ and with a flat "S"-shape is observed in the isotherms of CT-2 and CT-4, which belongs to the type-B hysteresis loop, suggesting that the presence of slit-like pores in the samples. Fig. 2(b) shows the pore size distributions curve calculated by the BJH method from the desorption branch of a nitrogen isotherm. It can be seen that all the porous CdS/TiO_2 samples contained two different levels of pores. For the CT-2 sample, the small micropores are centered at 1.88 nm, and the large mesopores with broadened pore size distribution are in the range of 2.14–5.46 nm. However, a further increase of the Ti:Cd molar ratio to 1:1.5, the pore size distribution of CT-4 sample slightly decreased, which contained small micropores (centered at1.84 nm) and large mesopores with a pore diameter range of 2.0–5.0 nm. These results clearly show that the as-prepared CdS/TiO_2 have a very clear hierarchically porous structure, and the porosity should be as a result of the organized aggregation of CdS/TiO_2 nanoparticles that formed by weak coordination interactions during the solvothermal reaction. In addition, the BET surface area and total pore volume are summarized in Table 1. It can be seen that the CT-2 sample shows a large BET surface area (134.9 m^2/g) and pore volume (0.159 m^3/g), which are all much higher than these of CT-4 sample. The results indicate that the higher specific surface area could be attributed to the preservation of hierarchical porous structure in CdS/TiO_2 samples.

The morphologies of the hierarchically porous CdS/TiO_2 heterojunctions were investigated using scanning electron microscopy (SEM), and the corresponding SEM images are shown in Fig. 3. It is clear that all of the obtained materials exhibit large aggregates formed by the accumulation of CdS/TiO_2 nanoparticles, and some microspheres (O_1–O_3 with average diameter of approximately 1(±0.5) μm) and rod (flake)-like powders (S_1–S_3 with approximately 2(±0.5) μm in length) are well dispersed over the surface of hierarchically porous CdS/TiO_2 samples, which could provide more reactive sites for the reactants than aggregated particles. Some porosity is evident in the aggregation, which may serve as transport paths for small organic compound molecules or improve the catalytic performance because the hierarchically porous structure offering an effective pathway for the transportation of the charge carries.

The crystalline structure of hierarchically porous CdS/TiO_2 sample was examined with a high resolution transmission electron microscope (HR-TEM). Fig. 4 shows the typical HR-TEM image of CT-2 sample. The well-resolved two-dimensional lattice fringes of the material can be observed clearly, indicating a high crystallization degree of hierarchically porous CdS/TiO_2 sample. The interplanar spacing was measured carefully from the lattice fringes and compared with the data in JCPDS, and the value with 0.352 nm and 0.335 nm can be indexed to the (1 0 1) facet in anatase TiO_2 [31] and the (0 0 2) inter-plane of hexagonal CdS [32], respectively. It also can be observed from Fig. 4 the particle size of CdS and

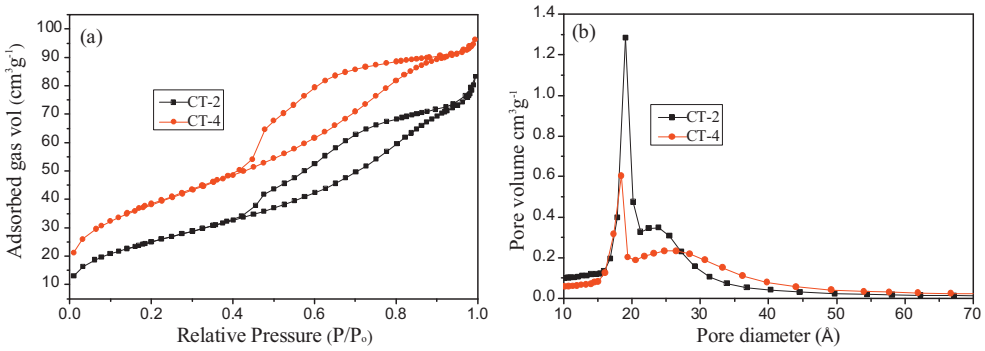

Fig. 2. (a) Nitrogen adsorption–desorption isotherms and (b) the corresponding pore size distributions curve of the hierarchically porous CdS/TiO_2 heterojunction.

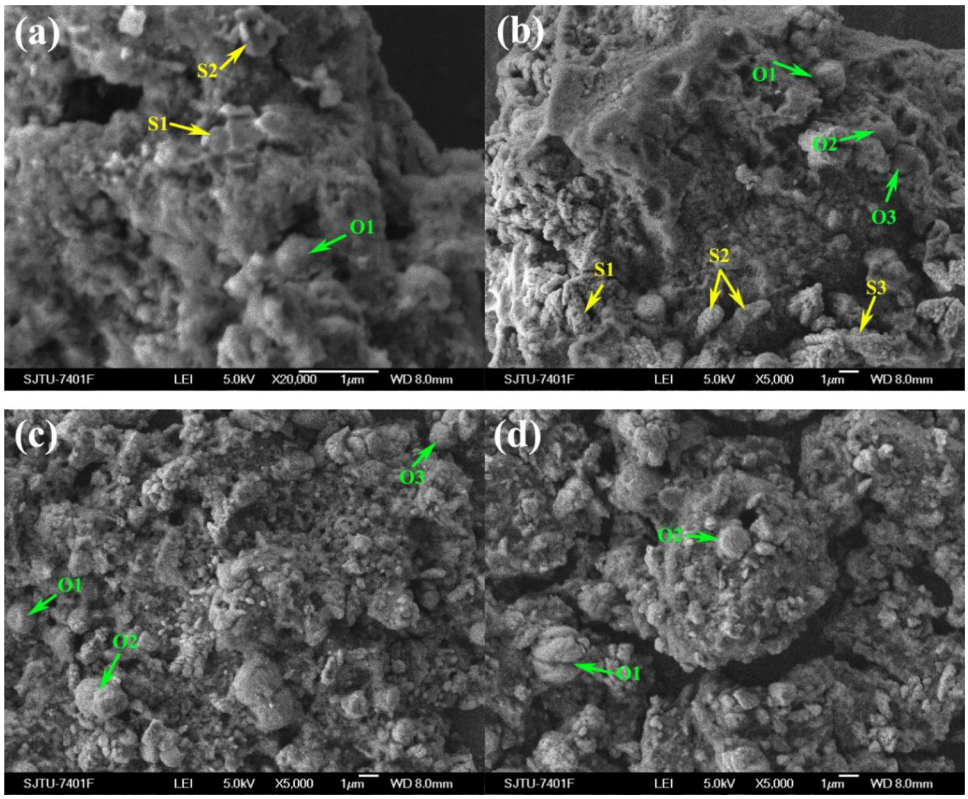

Fig. 3. SEM image of the hierarchically porous CdS/TiO_2 heterojunction samples with different Ti:Cd molar ratios. (a) CT-1, (b) CT-2, (c) CT-3, and (d) CT-4.

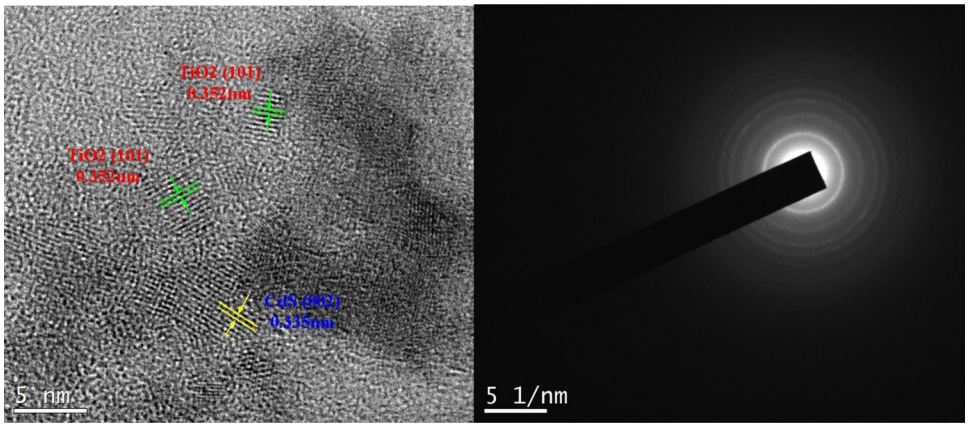

Fig. 4. High resolution TEM image and SAED pattern of CT-2 sample.

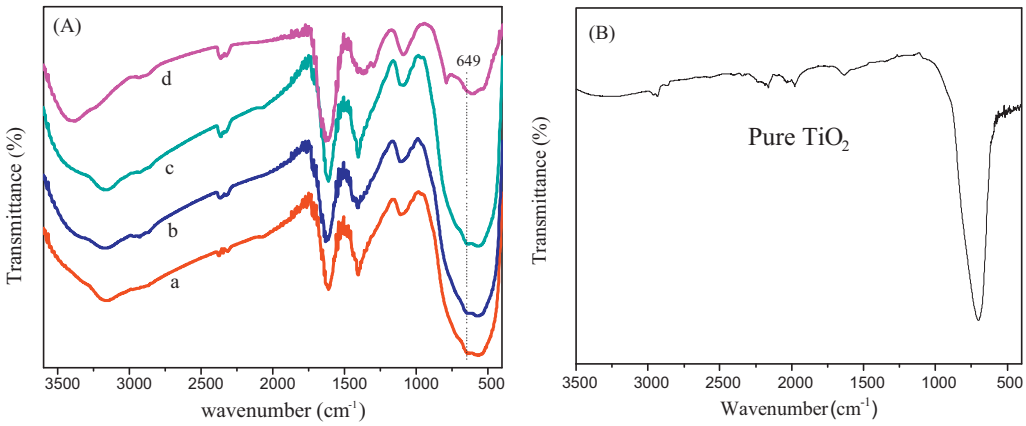

Fig. 5. FT-IR spectra of hierarchically porous CdS/TiO_2 heterojunction samples. (A) (a) CT-1, (b) CT-2, (c) CT-3, and (d) CT-4. (B) FT-IR spectra of pure TiO_2.

TiO_2 nanocrystals is about 6 and 4 nm, respectively. Furthermore, the selected area electron diffraction (SAED) pattern also demonstrates that the hierarchically porous heterojunctions are the result of the self-assembly of smaller cadmium sulphide and titanium oxide nanocrystals. These results further confirm that an individual CdS nanoparticle is closely attached on the TiO_2 nanoparticle and the formation of distinct juncture between two crystal phases in the CdS/TiO_2 system, which is in accordance with the XRD analysis.

Fig. 5(A) shows the FT-IR spectra of hierarchically porous CdS/TiO_2 heterojunction samples with varying molar ratios of titanium to cadmium, and the data for the pure TiO_2, used here as a reference, is shown in Fig. 5(B). The FT-IR spectra reveal that all the as-prepared CdS/TiO_2 and pure TiO_2 samples present absorbance bands around 3400 and 1630 cm^{-1}, which can be ascribed to the absorbed surface hydroxyl (water molecular) and the O—H bending vibration [33], respectively. The broad peak in the region of 400–800 cm^{-1} is due to the Ti—O stretching and Ti—O—Ti bridging stretching modes [4,34]. To carefully compare the FT-IR spectra of the CdS/TiO_2 and the pure TiO_2 sample, it is found that the CdS/TiO_2 heterojunction samples display an additional satellite peak located at 649 cm^{-1}, which can be attributed to Cd—S stretching [34,35]. This result reveals that CdS molecules are attached to TiO_2.

Fig. 6 shows the UV–vis diffuse reflectance spectra of hierarchically porous CdS/TiO_2 photocatalysts prepared using the one-step solvothermal method. The inset of Fig. 6 shows the UV–vis diffuse reflectance spectrum for pure TiO_2. It is seen that pure TiO_2 sample exhibits no optical absorption in visible light region due to its big energy band gap (3.2 eV). All of the hierarchically porous CdS/TiO_2 heterojunction samples show a higher absorption both in the visible light area and near infrared region, indicating that the visible light response of CdS/TiO_2 materials mainly resulted from the synergistic photosensitization of CdS and remnant carbonaceous precursor rather than the formation of hybrid energy levels [18]. The results are also consistent with the physical appearance of the dark yellow CdS/TiO_2 powders. It is worth noting that the optical absorption is not linearly changed to CdS coupling. As expected, the as-prepared CdS/TiO_2 heterojunctions have great photocatalytic activity under visible light irradiation. Because the CdS has a narrow energy band gap, which can be used to harvest the most of visible light, and thus the electrons can be excited to inject electrons into the conduction band of TiO_2, leading to the improvement of electron–hole pair separation.

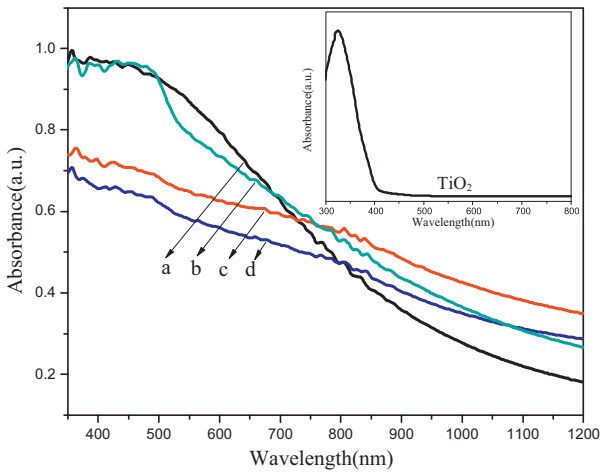

Fig. 6. UV–vis diffuse reflectance spectra of hierarchically porous CdS/TiO_2 heterojunction samples. (a) CT-1, (b) CT-2, (c) CT-3, and (d) CT-4.

The surface element composition of the as-prepared hierarchically porous CdS/TiO_2 photocatalyst and the chemical states of elements (e.g. Cd, S, Ti and O) in the samples were analyzed using XPS analysis. Fig. 7 shows the XPS spectrum of CT-2 sample, and all binding energies were calibrated using the contaminant carbon (284.8 eV) as the reference. As can be seen from the whole XPS survey spectra for CT-2 (Fig. 7a), all the peaks due to the C, Cd, S, Ti and O elements were observed in the spectra at binding energies around 285, 405, 162, 459 and 531 eV, respectively, suggesting that the sample was composed of C, Cd, S, Ti and O elements. It should be noted that the XPS peak for C1s is due to the remaining carbonaceous species formed during the preparation.

Fig. 7b gives the Cd3d XPS spectra of CT-2. There are two peaks at binding energies 404.9 and 411.6 eV, which can be assigned to $Cd3d_{3/2}$ and $Cd3d_{5/2}$, respectively, indicative of Cd^{2+} in the CdS/TiO_2 composite [36]. It is also found that the difference between the binding energies of $Cd3d_{5/2}$ and $Cd3d_{3/2}$ peaks is 6.7 eV, which further confirms that the presence of characteristic +2 Cd3d states on the sample surface. Fig. 7c shows the S2p XPS spectra for CT-2. It can be seen that the S2p peak is broad and asymmetric, and the peak can be fitted with three peaks at 163.7, 162.2 and 161.0, suggesting three independent S species are present in CT-2 sample. The peak's position corresponding to $S2p_{1/2}$ and $S2p_{3/2}$ is at 161.0 and 162.2 eV, which indicated that S element exists mainly in the form of S^{2-} chemical state on the sample surface. Furthermore, the 1.2 eV difference between the binding energies of $S2p_{1/2}$ and $S2p_{3/2}$ is also characteristic of −2S in CdS [37], whilst the fitting peak at the binding energy of 163.7 eV is attributed to the surface Ti—S bonds formed when some of the oxygen atoms in the TiO_2 lattice are replaced by the S atom [38].

From the XPS spectrum of Ti2p (Fig. 7d), the binding energies of $Ti2p_{3/2}$ and $Ti2p_{1/2}$ in the material are 459.0 and 464.6 eV,

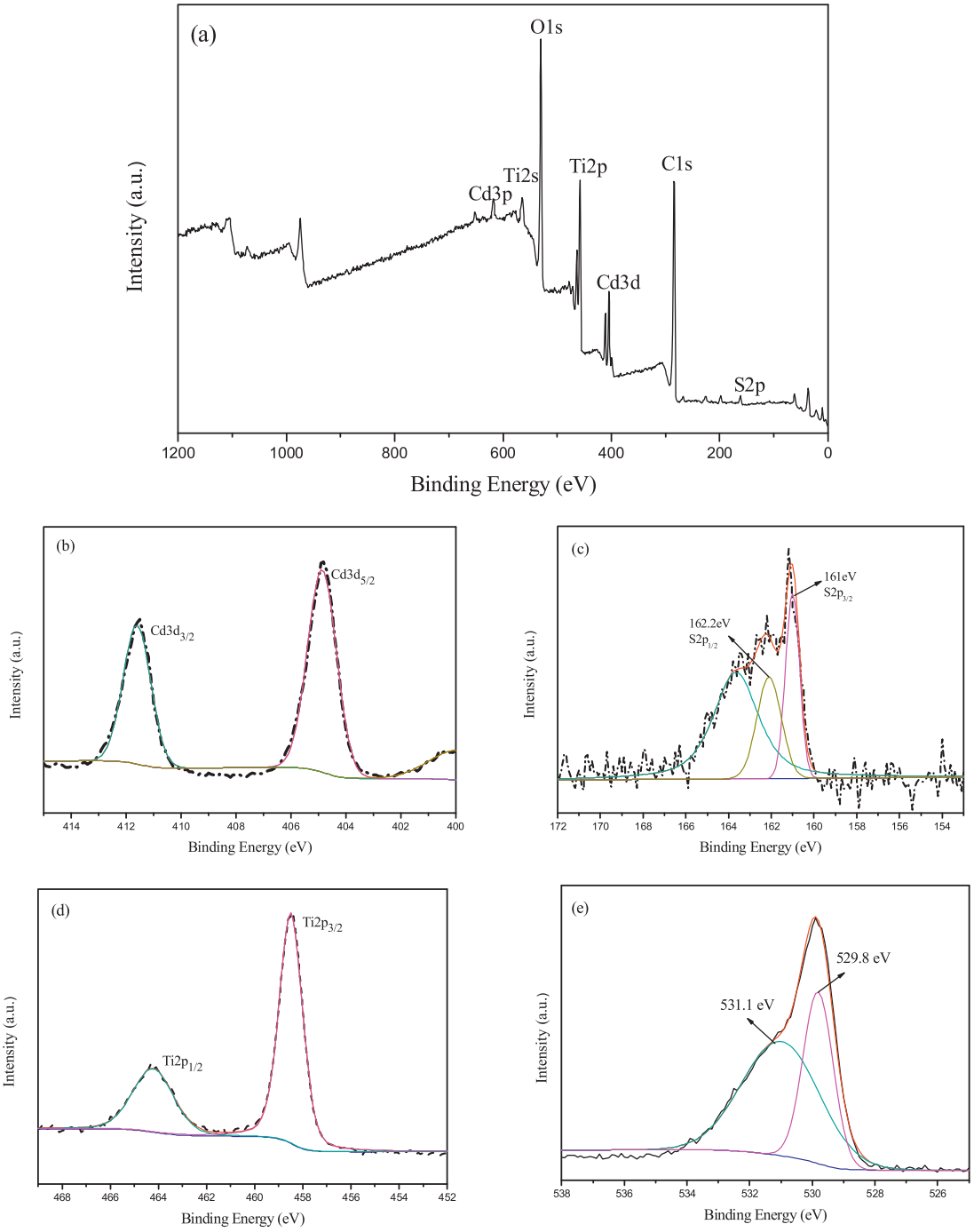

Fig. 7. XPS spectra of CT-2 sample. (a) The survey spectra of CdS/TiO_2 heterojunction, (b) Cd3d XPS spectra, (c) S2p XPS spectra, (d) Ti2p XPS spectra, and (e) O1s XPS spectra.

respectively. These data are in agreement with previously reported by our research and which arises from the presence of Ti^{4+} on the surface of CdS/TiO_2 heterojunction [39]. Fig. 7e shows an O1s XPS spectrum of CT-2, with the asymmetric peak located around 530.0 eV, indicating there are at least two kinds of oxygen species existing on the sample surface. The curve fitting patterns are also shown in Fig. 7e. The high binding energy of around 531.1 eV can be assigned to the oxygen of surface hydroxyl. Meanwhile the other peak located at 529.8 eV is due to the lattice oxygen of TiO_2 [15].

It is well known that the methyl orange is a very stable azo dye and cannot be degraded under visible light [40], except when assisted by an appropriated photocatalyst. In the current work, the MO solution of 10 mg/L was used as the model pollutant to evaluate the photocatalytic activity of the hierarchically porous CdS/TiO_2 heterojunction samples under visible light illumination. Fig. 8 shows the corresponding plot for the change of MO concentration determined from its characteristic absorption peak at 464 nm. For comparison, the photodegradation efficiencies of methyl orange over pure TiO_2 as well as without photocatalyst (photolysis of MO) are also shown in Fig. 8. The blank test shows that the MO does not degrade in the absence of catalyst, while less than 1% photocatalytic efficiency of pure TiO_2 can be observed within 120 min visible light irradiation, indicating that the pure TiO_2 has no visible light activity due to its big energy band gap. However, all the as-prepared hierarchically porous CdS/TiO_2 materials exhibit much higher photocatalytic activity than the pure TiO_2, because

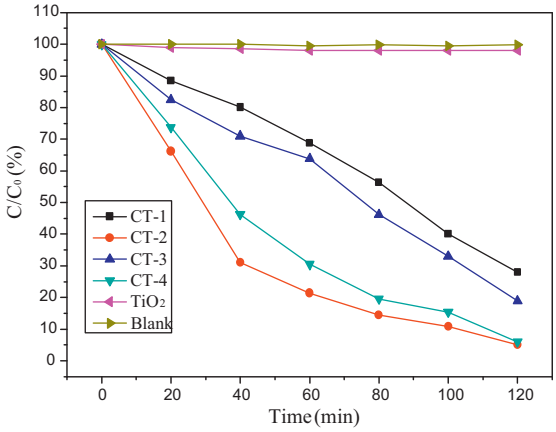

Fig. 8. The decomposition curves of MO solution by hierarchically porous CdS/TiO_2 heterojunction samples under visible light irradiation ($\lambda \geq 420$ nm). The concentration of MO is solution 10 mg/L.

the incorporation of CdS extends the absorption to the visible light region. Among all photocatalysts evaluated, the CT-2 sample displays the highest potocatalytic activity, and the decomposition rate of MO solution reaches the maximum value of 95% within 120 min visible light irradiation. Furthermore, the photodegradation efficiencies of CT-1, CT-3 and CT-4 samples are about 72%, 81% and 94%, respectively. As can be seen that the apparent activity sequence of the heterojunctions is related to the CdS coupling content, the degradation rate order of all the samples is as follow: CT-2 > CT-4 > CT-3 > CT-1> pure TiO_2.

In order to further examine the photocatalytic performance of the obtained CdS/TiO_2 hierarchical heterojunctions, the photodegradation experiments for decoloration of 20 mg/L rhodamine B solution over these samples were also carried out under the same conditions. As mentioned earlier [41,42], the RhB as one of the most widely used xanthenes dye for textile industry, which had high chemical stability and showed a characteristic absorption band at 554 nm. Fig. 9 shows the results for the degradation of RhB solution versus reaction time under visible light irradiation. It can be seen that without catalyst the concentration of RhB remains unchanged even after 140 min of visible light illumination, while all the as-prepared hierarchically porous CdS/TiO_2 heterojunctions as well as pure CdS hierarchical structure display a better visible-light-induced photocatalytic activity. Obviously, the CT-2 shows the best catalytic performance among all the five samples with nearly 85%

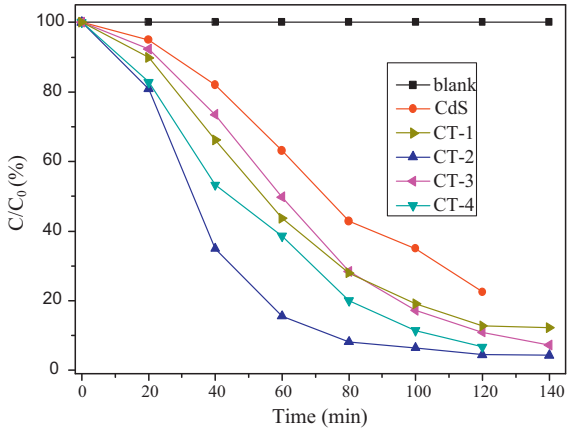

Fig. 9. The decomposition curves of RhB solution by hierarchically porous CdS/TiO_2 heterojunction samples under visible light irradiation ($\lambda \geq 420$ nm). The concentration of RhB solution is 20 mg/L.

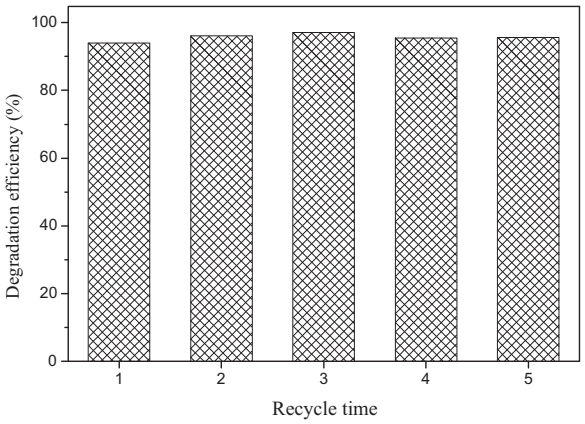

Fig. 10. Recycling test of RhB photodegradation on CT-2 sample under visible light irradiation (photoreaction time = 100 min).

RhB decomposed in the initial 60 min irradiation, and Fig. S1 also confirms that the RhB solution can be completely discolored over CT-2 sample within 140 min of visible light irradiation. Moreover, after 120 min of photoreaction, the values of decomposed RhB are, respectively, 87%, 89%, 93% and 77% for CT-1, CT-3, CT-4 and CdS. These results indicated that the photocatalytic activity of CdS/TiO_2 samples is associated with the loading amount of CdS, but is not linearly changed to CdS loading.

Supplementary material related to this article can be found, in the online version, at http://dx.doi.org/10.1016/j.apsusc.2013.06.122.

Besides the higher photoactivity, the hierarchically porous CdS/TiO_2 heterojunctions also show strong stability and reusability during the experiments of visible-light-driven photodegradation of RhB. As shown in Fig. 10, after five cycling photocatalysis reactions, the CT-2 sample still keeps its activity, and which can lead to the complete decomposition of the RhB solution under 100 min visible light irradiation.

As described above, the photocatalytic activities of all the hierarchically porous CdS/TiO_2 heterojunction samples for both the degradation of MO and RhB solution were significantly enhanced compared to the pure CdS and TiO_2, and the sample synthesized with the Ti:Cd molar ratio of 1:1 displays the highest activity under visible light irradiation, suggesting that coupling TiO_2 with CdS is an effective way to improve the degradation efficiency of the as-prepared photocatalysts owing to the formation of the junctions between the two individual components. According to the earlier reports and our experimental results [43,44], the electronic band structure of the heterojunctions plays a vital role in the determining the excitation, transportation and ultimate rate of charge carriers, as well as the photocatalytic activity. It is well known that the CdS is one of relatively smaller band gap semiconductor, which has more negative conduction band (CB) top and valence band (VB) bottom than TiO_2 [43]. As shown in the schematic diagram (Fig. 11), the band position of CdS and TiO_2 fit basic requirements to form a "staggered" type II heterojunction at the interface of the hybrid semiconductor. This type II band alignment can easily transfer the photogenerated electron from the conduction band of CdS to a TiO_2 molecule due to the presence of energy bias on the intimate contact interfaces between CdS and TiO_2. Such charge transfer could effectively separate electron–hole (e^-–h^+) pairs and inhibit their recombination, it therefore prolongs life time of these charge carriers, as a result of leading to the increased quantum efficiency.

On the other hand, the stronger visible light absorption of CdS/TiO_2 composite also contributes to the improvement of the photocatalytic decomposition of model pollutant, and which could increase the number of photogenerated electrons and holes able to

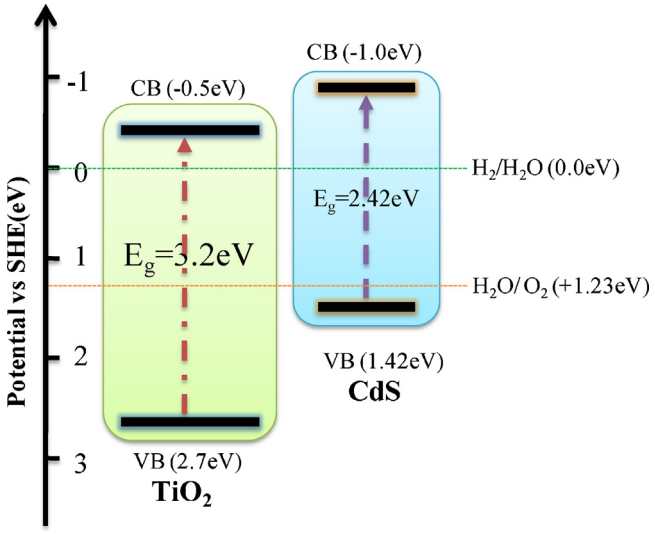

Fig. 11. Schematic electronic band diagram of the CdS/TiO_2 system.

participate in the photoreaction. In addition, the enhancement of the photocatalytic activity has been correlated with the larger specific surface area and total pore volume of the CdS/TiO_2 hierarchical heterostructures prepared by one-step solvothermal method. As indicated by BET measurement, CdS/TiO_2 samples with high surface area and total pore volume can provide more effective active sites and favor the increase of the amount of adsorbed dye molecules [41,44], which help to reduce the recombination of electron and hole, and result in a better catalytic performance. On the basis of the above discussions, it is therefore concluded that the increase of the photoactivity of the obtained samples can be attributed to the synergistic effect of the hybrid structure, larger surface area, hierarchical pores and strong visible light absorption.

4. Photocatalytic mechanism

As we have known, the as-prepared hierarchically porous CdS/TiO_2 heterojunction samples show the excellent photoactivity in the degradation of methyl orange and rhodamine B, indicating that the samples might have potential applications in the cleanup of environment. In order to further guide the improvement of the photocatalytic performance, we have also attempted to explore the mechanism of photocatalytic oxidation of organic compounds by the CdS/TiO_2 heterojunction. Fig. 12 presents the schematic diagram of the separation of generated electrons and holes on the interface of CdS/TiO_2 under visible light irradiation. In the hybrid system, CdS can be excited firstly under visible light irradiation to produce the electron–hole pairs due to its narrow energy band gap of 2.42 eV, and then the photo-excited electron on the CB of CdS would prefer to migrate to the CB of TiO_2 crossing the interface because the CB edge level of TiO_2 is more positive than that of CdS. Meanwhile the photogenerated hole on the VB of CdS would flow down to surface of CdS nanoparticles. It can be seen in this process that the recombination between electrons and holes is subsequently reduced, resulting in higher concentration of charges on the solid surface, and thus these charges (e^- and h^+) would have more opportunities for participating in decolorized reaction. As depicted in Fig. 12, the electrons existed in TiO_2 could reduce surface-absorbed oxygen over titanium dioxide active sites to form superoxide radical ($O_2^{\bullet -}$) and hydrogen peroxide (H_2O_2), and then these new species can interact to yield the hydroxyl radical (•OH) [45], which are responsible for the oxidative decomposition of organic pollutant.

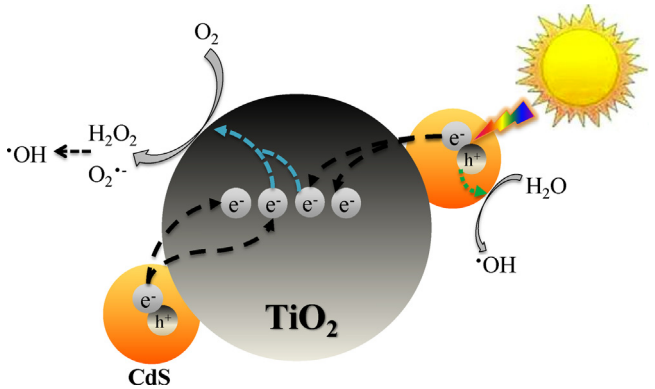

Fig. 12. Schematic diagram of the separation of generated electrons and holes on the interface of CdS–TiO_2 under visible light irradiation.

On the other hand, the holes existed in CdS are also favorable for the photo-oxidation of organic compounds, and two different fundamental oxidation mechanisms are proposed as follows: First, due to the stronger oxidation potential, the holes themselves can directly oxidize both MO and RhB molecules, and this could be considered as the dominant pathway because the absorption of a large number of organic compounds over CdS/TiO_2 surface is the prerequisite step for the photoreaction. Second, the holes could potentially react with the surface-absorbed H_2O at active sites to generate hydroxyl radical (•OH) [36,46], which can then attack the dye molecules and finally induce the decomposition of organic substrates effectively. In the case of our experiment, it is thought that both direct oxidation by hole and indirect oxidation by hydroxyl radical have to be operative simultaneously to produce the best overall oxidation results.

5. Conclusion

CdS/TiO_2 heterojunctions with hierarchically porous structure were successfully synthesized by one-step solvothermal method at low temperature. The obtained photocatalysts were characterized by XRD, SEM, HRTEM, UV–vis DRS, XPS and N_2 adsorption–desorption. The results show that the hexagonal CdS has been attached to the anatanse TiO_2 nanoparticles to form the heterostructure with larger specific surface area and higher pore volume. The photocatalytic activity of CdS/TiO_2 heterojunction was assessed for degradation of both MO and RhB under visible light irradiation, and all the as-prepared samples exhibit enhanced photocatalytic performance due to the increase of specific surface area for more absorbed dyes, the electronic band structure and the additional synergistic effect within junctions between CdS and TiO_2, which could effectively inhibit the recombination of photoexcited electron–hole pairs.

Acknowledgements

This work was financially supported by the Fundamental Research Funds for the Central Universities (Grant No. 2012jdhz40) and the Overall Scientific and Technological Innovation Program of Shaanxi Province of China (No. 2012KTCL01-09).

References

[1] D.V. Bavykin, J.M. Friedrich, F.C. Walsh, Adv. Mater. 18 (2006) 2807–2824.
[2] Z. He, Y. Li, Q. Zhang, H. Wang, Appl. Catal. B: Environ. 93 (2010) 376–382.
[3] A. Fujishima, K. Honda, Nature 238 (1972) 37–38.
[4] G. Yang, Z. Jiang, H. Shi, M.O. Jones, T. Xiao, P.P. Edwards, Z. Yan, Appl. Catal. B: Environ. 96 (2010) 458–465.
[5] S. Liu, J. Yu, M. Jaroniec, J. Am. Chem. Soc. 132 (2010) 11914–11916.

[6] J. Ye, W. Liu, J. Cai, S. Chen, X. Zhao, H. Zhou, L. Qi, J. Am. Chem. Soc. 133 (2011) 933–940.
[7] T.R. Gordon, M. Cargnello, T. Paik, F. Mangolini, R.T. Weber, P. Fornasiero, C.B. Murray, J. Am. Chem. Soc. 134 (2012) 6751–6761.
[8] G. Yang, T. Xiao, J. Sloan, G. Li, Z. Yan, Chem. Eur. J. 17 (2011) 1096–1100.
[9] A.K. Benabbou, Z. Derriche, C. Felix, P. Lejeune, C. Guillard, Appl. Catal. B: Environ. 76 (2007) 257–263.
[10] J. Du, W. Chen, C. Zhang, Y. Liu, C. Zhao, Y. Dai, Chem. Eng. J. 170 (2011) 53–58.
[11] Y. Cao, T. He, L. Zhao, E. Wang, W. Yang, Y. Cao, J. Phys. Chem. C 113 (2009) 18121–18124.
[12] G. Yang, Z. Yan, T. Xiao, Appl. Surf. Sci. 258 (2012) 4016–4022.
[13] A. Zaban, S. Ferrere, J. Sprague, B.A. Gregg, J. Phys. Chem. B 101 (1997) 55–57.
[14] S.C. Hayden, N.K. Allam, M.A. Ei-Sayed, J. Am. Chem. Soc. 132 (2010) 14406–14408.
[15] G. Yang, Z. Yan, T. Xiao, Appl. Surf. Sci. 258 (2012) 8704–8712.
[16] L. Ge, J. Liu, Appl. Catal. B: Environ. 105 (2011) 289–297.
[17] L.-C. Chen, F.-R. Tsai, S.-H. Fang, Y.-C. Ho, Electrochim. Acta 54 (2009) 1304–1311.
[18] Y. Huo, X. Yang, J. Zhu, H. Li, Appl. Catal. B: Environ. 106 (2011) 69–75.
[19] R. Ahmed, G. Will, J. Bell, H. Wang, J. Nanopart. Res. 14 (2012) 1140.
[20] Y.-J. Chi, H.-G. Fu, L.-H. Qi, K.-Y. Shi, H.-B. Zhang, H.-T. Yu, J. Photochem. Photobiol. A 195 (2008) 357–363.
[21] P. Yang, T. Deng, D. Zhao, P. Feng, D. Pine, B.F. Chmelka, G.M. White-sides, G.D. Stucky, Science 282 (1998) 2244–2246.
[22] X. Wang, J.C. Yu, C. Ho, Y. Hou, X. Fu, Langmuir 21 (2005) 2552–2559.
[23] G.-S. Shao, X.-J. Zhang, Z.-Y. Yuan, Appl. Catal. B: Environ. 82 (2008) 208–218.
[24] G. Hasegawa, K. Kanamori, K. Nakanishi, T. Hanada, J. Am. Ceram. Soc. 93 (2010) 3110–3115.
[25] J.H. Pan, X. Zhang, A.J. Du, D.D. Sun, J.O. Leckie, J. Am. Chem. Soc. 130 (2008) 11256–11257.
[26] Z.-D. Meng, M.-M. Peng, L.W.-C. Zhu, Oh F.-J. Zhang, Appl. Catal. B: Environ. 113–114 (2012) 141–149.
[27] H. Gerischer, M. Lubke, J. Electroanal. Chem. 204 (1986) 225–227.
[28] J.C. Colmenares, M.A. Aramendia, A. Marinas, J.M. Marinas, F.J. Urbano, Appl. Catal. A 306 (2006) 120–127.
[29] K.S.W. Sing, D.H. Everett, R.A.W. Haul, L. Moscou, R.A. Pier-otti, J. Rouquerol, T. Siemieniewska, Pure Appl. Chem. 57 (1985) 603–619.
[30] J.C. Yu, L. Zhang, J. Yu, Chem. Mater. 14 (2002) 4647–4653.
[31] T. Lv, L. Pan, X. Liu, T. Lu, G. Zhu, Z. Sun, C.Q. Sun, Catal. Sci. Technol. 2 (2012) 754–758.
[32] N.A. Razik, J. Mater. Sci. Lett. 6 (1987) 1443–1444.
[33] Y. Huo, Y. Jin, J. Zhu, H. Li, Appl. Catal. B: Environ. 89 (2009) 543–550.
[34] S.S. Mali, S.K. Desai, D.S. Dalavi, C.A. Betty, P.N. Bhosale, P.S. Patil, Photochem. Photobiol. Sci. 10 (2011) 1652–1658.
[35] T.P. Martin, H. Schaber, Spectrochim. Acta Part A 38 (1982) 655–660.
[36] F. Xu, Y. Yuan, H. Han, D. Wu, Z. Gao, K. Jiang, CrystEngComm 14 (2012) 3615–3622.
[37] L. Qi, J. Yu, M. Jaroniec, Phys. Chem. Chem. Phys. 13 (2011) 8915–8923.
[38] J. Yu, M. Zhou, B. Cheng, X. Zhao, J. Mol. Catal. A: Chem. 246 (2006) 176–184.
[39] G. Yang, Z. Jiang, H. Shi, T. Xiao, Z. Yan, J. Mater. Chem. 20 (2010) 5301–5309.
[40] Y. Li, X. Li, J. Li, J. Yin, Water Res. 40 (2006) 1119–1126.
[41] J.-W. Shi, X. Yan, H.-J. Cui, X. Zong, M.-L. Fu, S. Chen, L. Wang, J. Mol. Catal. A: Chem. 356 (2012) 53–60.
[42] M.-S. Gui, W.-D. Zhang, Y.-Q. Chang, Y.-X. Yu, Chem. Eng. J. 197 (2012) 283–288.
[43] D. Kannaiyan, E. Kim, N. Won, K.W. Kim, Y.H. Jang, M.-A. Cha, D.Y. Ryu, S. Kim, D.H. Kim, J. Mater. Chem. 20 (2010) 677–682.
[44] Y. Chen, D.D. Dionysiou, J. Mol. Catal. A 244 (2006) 73–82.
[45] G. Yang, Z. Yan, T. Xiao, B. Yang, J. Alloys Compd. 580 (2013) 15–22.
[46] W.Z. Tang, C.P. Huang, Water Res. 29 (1995) 745–756.